

## NUMERICAL STUDY ON THE FLOW PAST A FINITE-LENGTH TAPERED CYLINDER

by

**Shifeng WANG<sup>a</sup>, Kaixuan ZHENG<sup>b\*</sup>, and Deming NIE<sup>b</sup>**

<sup>a</sup>Science and Technology Department, Hangzhou Vocational and Technical College,  
Hangzhou, China

<sup>b</sup>Institute of Fluid Mechanics, China Jiliang University, Hangzhou, China

Original scientific paper  
<https://doi.org/10.2298/TSCI22S1131W>

*In this study, the flow past a finite-length tapered cylinder is numerically investigated via the finite-volume method with Reynolds numbers ranging from 50-250 and taper ratio  $\lambda = 1.5$ . The corresponding lift and drag coefficients, as well as the Strouhal numbers are presented. The factors related to the discontinuity, through Reynolds numbers of 100 – 200, in the lift coefficient, which is related to the wake structure of the tapered cylinder, are explained. Furthermore, the influence of the wake structure on the discontinuity in the lift coefficient is discussed. Finally, a comparison of the Strouhal numbers between the circular cylinder and tapered cylinder at the same Reynolds number is performed.*

Key words: tapered cylinder, wake structure, drag coefficient, lift coefficient, Strouhal number

### Introduction

The flow past a tapered cylinder is relevant in several engineering fields. For example, in architectural design, vortex-induced oscillation of bridges and wind turbines, and large-scale vortex shedding could cause vortex-induced oscillations, which are considered reasonable during the design phase. In practical engineering applications, these structures are generally designed as tapered cylinders with varying diameters [1, 2]. Owing to their relevance to engineering and architecture, analyzing the lift and drag coefficients, Strouhal numbers, and wake structure of a finite-length tapered cylinder for different Reynolds numbers is of great importance to engineering and architecture [3, 4].

Considerable attention has been paid to the flow past circular cylinders, however, the difference between tapered cylinders and circular cylinders remains undiscussed [5-7]. The critical Reynolds numbers for the finite-length circular cylinder were approximately 55-60. The discontinuity in lift coefficient for circular cylinders occurs approximately at 60 Reynolds number. A previous study discussed whether end plates or simple free ends (ranging from 6 to 15 cylinder diameters in length) could decrease the frequency of the vortex-shedding mechanism near these boundaries (the frequency of vortex-shedding in finite circu-

---

\*Corresponding author, e-mail: s21020804080@cjlu.edu.cn

lar cylinders is 10-15% less than that in regulars) [8-11]. However, studies on the lift and drag coefficients, Strouhal numbers, and wake structure of finite-length tapered cylinders for different Reynolds numbers are limited [12-15]. Therefore, this study focuses primarily on the lift and drag coefficients, Strouhal numbers, and wake structure of a finite-length tapered cylinder with Reynolds number between 50 and 250, and a taper ratio  $\lambda = 1.5$ . Consequently, the differences between the circular cylinder and tapered cylinder at the same Reynolds number are discussed. Finally, the correlation between the discontinuity in the lift coefficient and wake structure modes of the tapered cylinder, in the range of  $Re = 100-200$ , is considered.

### Numerical method

Herein, the bottom surface diameter,  $d$ , of the tapered cylinder resided in a hexahedral domain, fig. 1. The free stream flow,  $U_0$ , was along the  $y$ -axis, whereas the axis of the cylinder was along the  $z$ -axis. The computational domain measured  $40d \times 30d \times 24d$ . The length of the tapered cylinder was  $h$ . The diameter of the bottom surface of the finite-length tapered cylinder was  $d$  and the diameter of the top surface was  $\lambda d$ . The upstream and downstream boundaries were located at distances of  $L_u$  and  $L_d$  from the center of the cylinder, respectively where  $H$  is the domain height. A uniform flow was prescribed on the upstream face. The pressure was set to zero at the outflow boundary. The bottom surface was set as a no-slip surface. The symmetry condition was used on all other walls of the computational domain, that is, the velocity component normal to that wall and the stress vector components in the plane of the wall were assigned zero values. The reported computations were performed with  $L_u = 12d$ ,  $L_d = 28d$ ,  $\lambda = 1.5$ ,  $h = 8d$ , and  $H = 16d$ .

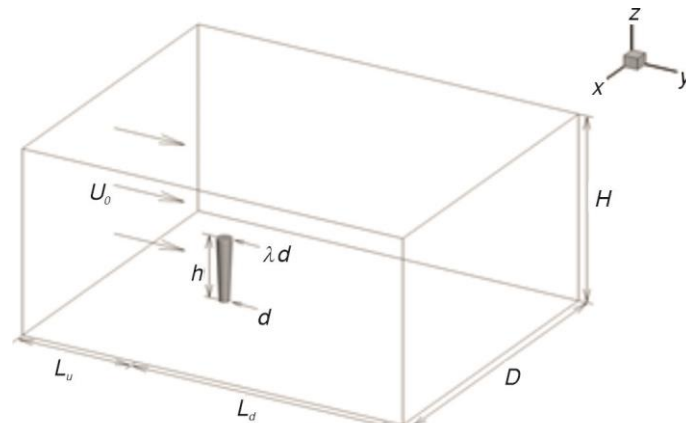


Figure 1. Computational domain

In this study, large-eddy simulation (LES) was adopted; accordingly, the implication of the Kolmogorov theory of turbulence is that smaller scales are more universal, whereas the large eddies in the flow are dependent on the geometry. The LES is a numerical method for integrating spatially filtered equations of motion that describe 3-D turbulence and high-Reynolds number time evolution. The central method in LES turbulence, in which smaller eddies are ignored in a turbulent flow simulation, is achieved by adopting a filtering equation to the full Navier-Stokes equations. The filtering operation in this model is achieved through a convolution operation with a filtering kernel. The general procedure for applying a filtering kernel to any function  $\phi$  is defined as follows [16]:

$$\overline{\phi(\mathbf{x}, t)} = \int_{-\infty}^{\infty} \int_{-\infty}^{\infty} \phi(\mathbf{r}, \tau) G(\mathbf{x} - \mathbf{r}, t - \tau) d\tau d\mathbf{r} \quad (1)$$

Time step: Appropriate step should be selected to satisfy the Courant-Friedrichs-Lewy condition using the equation:

$$C = \Delta t \sum_{i=1}^n \frac{u_i}{\Delta i} \leq C_{\max} \quad (2)$$

where  $C$  is the Courant number,  $C_{\max} = 1$ ,  $u_i$  – the flow velocity in the direction  $I$ ,  $\Delta i$  – the minimum computational grid size, and  $\Delta t$  is the computational time-step size. In this study,  $n = 1$  and  $C = 0.8$  are specified, and  $\Delta t = 0.01$  seconds, as calculated based on  $Re = 100$ , which satisfies the requirements.

Mesh irrelevance check: The adequacy of the spatial resolution was tested via computations on a finer mesh. Three sets of meshes with 15% increments in the number of cells were chosen from tab. 1 to compare Strouhal number at  $Re = 200$ , the results are reported. Evidently, the third case differed by only 1.815% from the second case of Strouhal number; therefore, the second case was chosen, fig. 2.

**Table 1. Irrelevance verification of cells**

Number of cells	Strouhal number	Error
$1.12 \times 10^6$	0.1201	
$1.29 \times 10^6$	0.1244	3.456%
$1.50 \times 10^6$	0.1267	1.815%

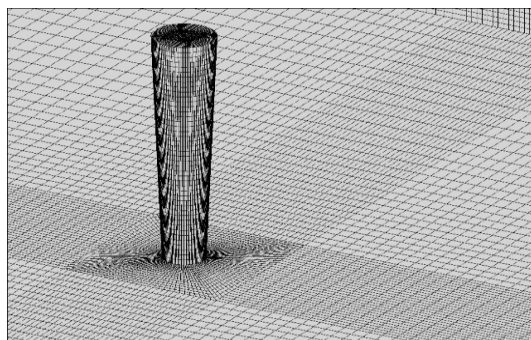


**Figure 2. The 3-D mesh consists of 1331824 nodes and 1295227 eight-node hexahedral elements**

## Numerical results

### *Drag and lift coefficients*

As shown in fig. 3 and tab. 2, the critical Reynolds number was between 65 and 70, which was higher than the critical Reynolds number of the finite-length cylinder,  $55 \leq Re \leq 60$ . Between  $Re = 70$  and  $Re = 100$ , a positive linear increase in the amplitude of  $C_l$  with an increase in Reynolds number was detected. Note that the discontinuity in  $C_l$ , for  $Re = 100$ –200, is associated with the inception of different wake modes. The difference between wake Modes 1 and 2 is the coupling between the upper and lower vortex loops in the finite-length tapered cylinder, which leads to the lift coefficient discontinuity. Additionally, the lift coefficients become increasingly non periodic.

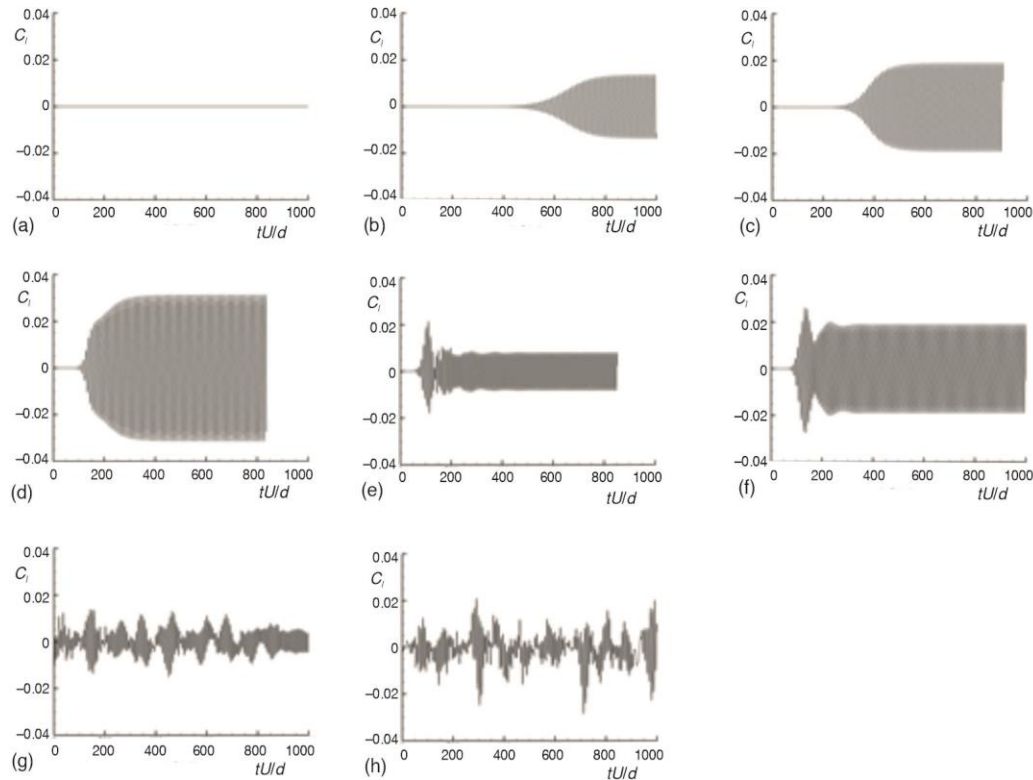


**Figure 3.** Time histories of lift coefficients at a various Reynolds number; (a)  $Re = 65$ , (b)  $Re = 70$ , (c)  $Re = 75$ , (d)  $Re = 100$ , (e)  $Re = 150$ , (f)  $Re = 200$ , (g)  $Re = 250$ , and (h)  $Re = 300$

**Table 2.** Variation in lift coefficient,  $C_l$ , amplitude with respect to Reynolds number

Reynolds number	Strouhal number	Amplitude of $C_l$
65	0	0
70	0.088	0.0139
75	0.090	0.0191
100	0.103	0.0315
150	0.115	0.0193
200	0.124	0.0083

Compared with the existence of two stages in the transition,  $Re = 170-180$  and  $Re = 230-260$ , to 3-D of a cylinder wake by Williamson [5, 12], the discontinuities in Strouhal number and  $C_l$  for the cylinder occurred at the same stage of the transition; in contrast, the discontinuity in  $C_l$  for the finite-length tapered cylinder occurred at the stage of  $Re = 100-200$ , but its discontinuity in Strouhal number occurred at the stage of  $Re = 300-400$ . Accordingly, this study focused on the discontinuity in  $C_l$  at  $Re = 70-100$ , which is discussed in more detail in present section and fig. 4.

The figure depicts a negative linear increase in the drag coefficient with an increase in Reynolds number. The drag coefficient gradually became unstable for  $Re > 200$ , which coincided with the non-periodic behavior of the lift coefficient.

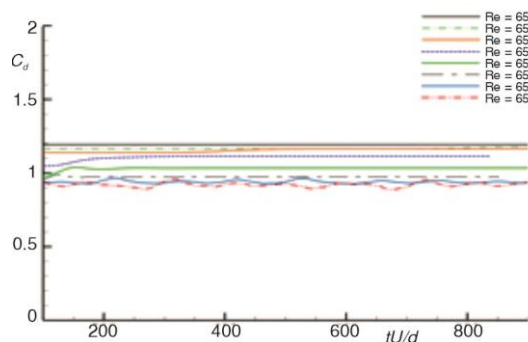


**Figure 4.** Time histories of drag coefficients at different Reynolds number for a round table

### Strouhal number

According to the experiments conducted by Detlev Gerich and Helmut Eckelmann [8], the free ends or end plates, ranging from 6 to 15 cylinder diameters in length, can decrease the frequency of the vortex-shedding mechanism near the boundaries, finite circular cylinder frequency of vortex-shedding 10-15% is less than of the regulars. Therefore, the Strouhal number of the tapered cylinder, which is less than that of the cylinder without free ends, is owing to the free end of the tapered cylinder and its taper ratio  $\lambda$ , tab. 3 and fig. 5 [12, 13, 17].

**Table 3.** Strouhal number with respect to different Reynolds number

Re	Finite length tapered cylinder (present) Strouhal number	Cylinder Williamson experiment [12] Strouhal number
70	0.087	0.145
75	0.091	0.148
100	0.103	0.164
150	0.114	0.185
200	0.127	0.184
250	0.131	0.197
300	0.134	0.203
400	0.135	0.206
500	0.129	—

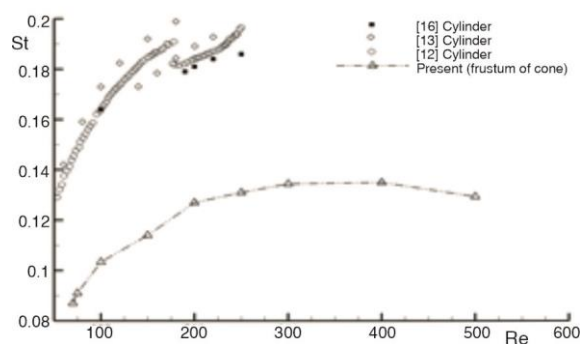


**Figure 5.** Variation in Strouhal number with respect to Reynolds number

### Wake structure

According to the coupling between the upper and lower vortex loops in the finite-length tapered cylinder, it is divided into two wake modes. Mode 1 – the upper vortex loop of the tapered cylinder is clearly demarcated from the lower vortex loop without coupling, as shown in fig. 6. Mode 2 – the upper and lower vortex loops are coupled, as shown in fig. 7.

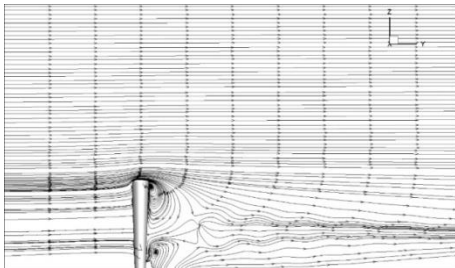


Figure 6. Streamlines for  $Re = 100$  and  $X = 16d$  at a specific time instant

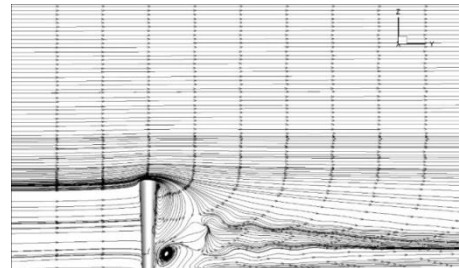


Figure 7. Streamlines for  $Re = 150$  and  $X = 16d$  at a specific time instant

As shown in fig. 9, the lift force was generated primarily by the pressure difference between the two sides of the finite-length tapered cylinder, and the pressure difference was concentrated primarily in the middle section. Essentially, the major difference between Modes 2 and 1 is whether the upper and lower vortex loops are coupled, and whether the streamline passing through the upper part of the wake is directly involved in the lower part of the wake. Second, as seen in figs. 8 and 9, the area covered by the upper part of the wake generated less lift force than that covered by the lower part of the wake, which resulted in the lift coefficient discontinuity/drop, between  $Re = 100$  and  $Re = 200$ .

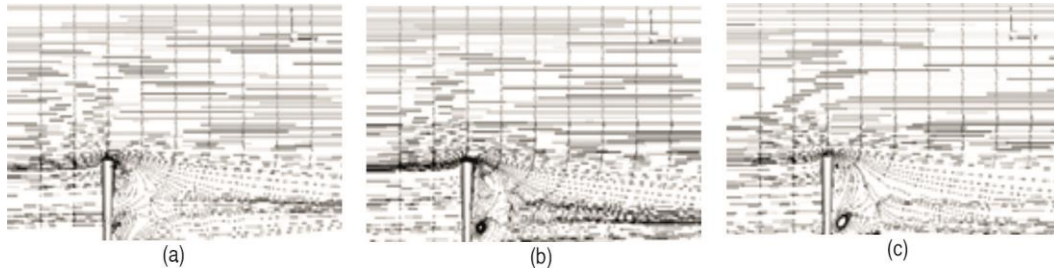


Figure 8. Streamlines for  $X = 16d$  and various Reynolds number at a specific time instant; (a)  $Re = 100$ , (b)  $Re = 150$ , and (c)  $Re = 200$

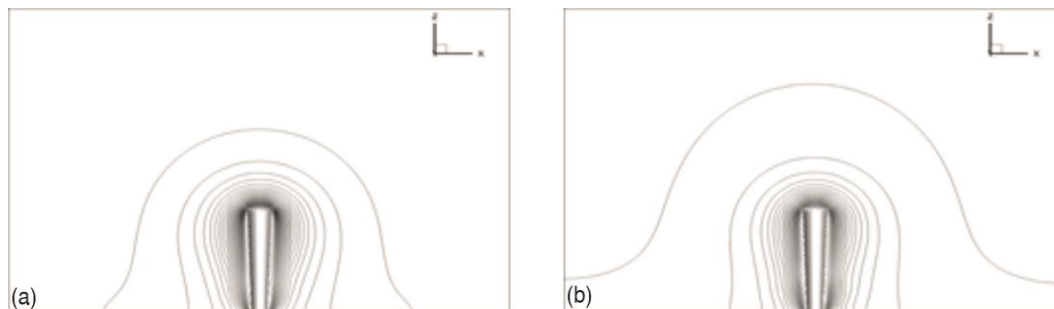


Figure 9. Pressure contours at  $Y = 12.375d$  for; (a)  $Re = 100$  and (b)  $Re = 150$

## Conclusion

- The critical Reynolds number of the tapered cylinder was between 65 and 70, which is higher than the critical Reynolds number of the finite-length cylinder,  $55 \leq \text{Re} \leq 60$ . Between  $\text{Re} = 70$  and  $\text{Re} = 100$ , we detected a positive linear increase in the amplitude of  $C_l$  with an increase in Reynolds number. The discontinuity in  $C_l$ , between  $\text{Re} = 100$  and  $\text{Re} = 200$ , is associated with the inception of different wake modes. The major differences between Modes 2 and 1 are whether the upper and lower vortex loops are coupled, the streamline passing through the upper part of the wake is directly involved in the lower part of the wake, and area covered by the upper part of the wake generates less lift force than that covered by the lower part of the wake, which leads to the lift coefficient discontinuity/drop.
- Both the regular and tapered cylinders exhibited a discontinuity in  $C_l$ , which is associated with the wake modes. However, the discontinuities in  $C_l$  and Strouhal number of the regular cylinder both occurred at the same Reynolds number, which is different from the  $C_l$  and Strouhal number of the tapered cylinder. The discontinuity in  $C_l$  of the tapered cylinder occurred at  $\text{Re} = 100$ -200, whereas the discontinuity of Strouhal number occurred at  $\text{Re} = 300$ -400, which is dislocated.
- According to the experiments conducted by Detlev Gerich and Helmut Eckelmann [3], the free ends or end plates, ranging from 6 to 15 cylinder diameters in length, could decrease the frequency of the vortex-shedding mechanism near the boundaries, finite circular cylinders frequency of vortex-shedding is 10-15% less than that of the regulars. Therefore, the Strouhal number of the tapered cylinder, which is less than that of the cylinder without free ends, is owing to the free end of the tapered cylinder and its taper ratio  $\lambda$ .
- The lift force was generated predominantly by the pressure difference between the two sides of the finite-length tapered cylinder, and the pressure difference was concentrated primarily in the middle section. The drag coefficient decreased with increasing Reynolds number because the denominator of the  $C_d$  calculation contained the square of the flow velocity. For  $\text{Re} > 200$ ,  $C_d$  gradually became unstable, which coincides with the non-periodic behavior of  $C_l$ .

## References

- [1] Ramesh, O. N., Chopde, R. S., Vortex Shedding Behind a Tapered Cylinder and Its Control, *Proceedings*, IUTAM Symposium on Flow Control and MEMS, London, UK, 2008
- [2] Kaja, K., et al., Three-Dimensional Numerical Simulations of Vortex-Induced Vibrations of Tapered Circular Cylinders, *Applied Ocean Research*, 60 (2016), Oct., pp. 1-11
- [3] Popov, S. G., Relation Between Strouhal and Reynolds Numbers for Two-Dimensional Flow About a Circular Cylinder, *Fluid Dynamics*, 1 (1966), Mar., pp. 107-109
- [4] Gonzalez, F. A., et al., Numerical Study of Flow Past Oscillatory Square Cylinders at Low Reynolds Number, *European Journal of Mechanics - B/Fluids*, 75 (2019), May-June, pp. 286-299
- [5] Williamson, C. H. K., The Existence of Two Stages in the Transition to Three-Dimensionality of a Cylinder Wake, *Physics of Fluids*, 31 (1988), 11, pp. 3165-3168
- [6] Behara, S., Mittal, S., Wake Transition in Flow Past a Circular Cylinder, *Physics of Fluids*, 22 (2010), 114104
- [7] Friehe, C., Vortex Shedding from Cylinders at Low Reynolds Numbers, *Journal of Fluid Mechanics*, 100 (1980), 2, pp. 237-241
- [8] Gerich, D., Eckelmann, H., Influence of End Plates and Free Ends on the Shedding Frequency of Circular Cylinders, *Journal of Fluid Mechanics*, 122 (1982), Sept., pp. 109-121
- [9] Konig, M., et al., Discrete Shedding Modes in the von Karman Vortex Street, *Physics of Fluids*, 5 (1993), 7, pp. 1846-1848

- [10] Stager, R., Eckelmann, H., The Effect of Endplates on the Shedding Frequency of Circular Cylinder in the Irregular Range, *Physics of Fluids*, 3 (1991), 9, pp. 2116-2121
- [11] Williamson, C. H. K., Oblique and Parallel Modes of Vortex Shedding in the Wake of a Circular Cylinder at Low Reynolds Numbers, *Journal of Fluid Mechanics*, 206 (1989), Sept., pp. 579-627
- [12] Williamson, C. H. K., Defining a Universal and Continuous Strouhal-Reynolds Number Relationship for the Laminar Vortex Shedding of a Circular Cylinder, *Physics of Fluids*, 31 (1988), 10, pp. 2742-2744
- [13] Zhang, H., *et al.*, On the Transition of the Cylinder Wake, *Physics of Fluids*, 7 (1995), 4, pp. 779-794
- [14] Tritton, D. J., A Note on Vortex Streets Behind Circular Cylinders at Low Reynolds Numbers, *Journal of Fluid Mechanics*, 45 (1971), 1, pp. 203-208
- [15] Seyed-Aghazadeh B., *et al.*, The Influence of Taper Ratio on Vortex-Induced Vibration of Tapered Cylinders in the Crossflow Direction, *Journal of Fluids and Structures*, 53 (2015), Feb., pp. 84-95
- [16] Persillon, H., Braza, M., Physical Analysis of the Transition to Turbulence in the Wake of a Circular Cylinder by Three-Dimensional Navier-Stokes Simulation, *Journal of Fluid Mechanics*, 365 (1998), June, pp. 23-88
- [17] Germano, M., *et al.*, A Dynamic Subgrid-Scale Eddy Viscosity Model, *Physics of Fluids*, 3 (1991), 7, pp. 1760-1765